IEEE Photonics Journal
An IEEE Photonics Society Publication

Study on VLC Channel Modeling Under Random Shadowing

Volume 9, Number 6, December 2017

Zanyang Dong
Tao Shang
Yan Gao
Qian Li

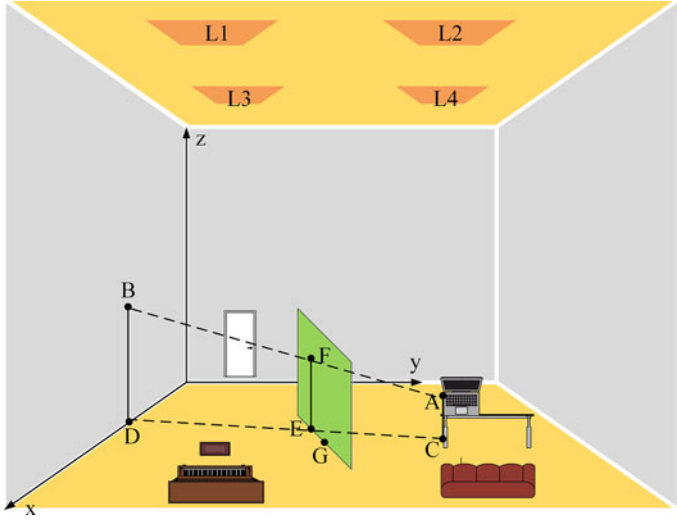

DOI: 10.1109/JPHOT.2017.2775664
1943-0655 © 2017 CCBY

IEEE photonics SOCIETY
IEEE

Study on VLC Channel Modeling Under Random Shadowing

Zanyang Dong,[1,2] **Tao Shang**,[1,2] **Yan Gao**,[1,3] **and Qian Li** [1,2]

[1]State Key Laboratory of Integrated Service Networks, School of Telecommunications EngineeringXidian University, Xi'an 710071, China
[2]Collaborative Innovation Center of Information Sensing and Understanding, Xidian University, Xi'an 710071, China
[3]Institute of China Electronic System Engineering Corporation, Beijing 100039, China

DOI:10.1109/JPHOT.2017.2775664

Manuscript received September 19, 2017; revised November 6, 2017; accepted November 16, 2017. Date of publication November 21, 2017; date of current version December 8, 2017. This work was supported in part by the 863 High Technology Plan of China under Grant 2013AA013402 and in part by the National Natural Science Foundation of China under Grants 61172080 and 61771357. Corresponding author: Tao Shang (email: shtsun_sjtu@hotmail.com).

Abstract: Recently, visible light communication (VLC) based on LEDs has attracted much attention. In order to realize multiusers indoor VLC systems, a reasonable channel model considering random shadowing, which is first proposed to the best of our knowledge, is significant. Taking the nonquantitative obstructions with random movement into account, by introducing the Poisson process and the probability density function, we propose a weighting function and set up a channel model. The expressions of the received optical power, the horizontal illuminance and the impulse responses are given. The verification of the model's feasibility is presented through simulation. Moreover, based on the proposed channel model, the simulation analysis of the effect of random shadowing on communication performance is conducted, and the corresponding simulation optimization is also made.

Index Terms: Visible light communication (VLC), channel model, random shadowing, weighting function.

1. Introduction

Recently, visible light communication (VLC) utilizing white LEDs has drawn considerable attention because of its multiple advantages such as less power consumption, high transmission rate, unlicensed spectrum, enhanced security, anti-electromagnetic interference and so on [1], [2]. For indoor VLC systems, full-duplex mode, multipath interference, multi-users access interference and networking schemes are research hotspots. To solve these problems, the reasonable channel model is significant for obtaining channel characteristics. As is known, almost all the VLC channel models [3]–[12] are developed from those of IR [13]–[17] by including wavelength dependent white LED characteristics and spectral reflectance of indoor reflectors. Particularly, in [10], the most realistic indoor VLC channel modeling is proposed for static scenarios by considering the presence of furniture and objects. The model presented in [10] has been endorsed by the IEEE 802.15.7r1 Task Group as the reference model [12]. However, for the VLC channel, the main concern should focus on not only the multipath effect due to many reflections, but also the effect of mobility and shadowing. In [9], the shadowing effect caused by the human body is considered for VLC channel characteristics. This however builds on some simplifying assumptions such as ideal Lambertian source and purely diffuse reflections. To address these issues, in [11], a realistic VLC channel model assuming a

mobile user is proposed. To demonstrate the benefits of link adaptation over a mobile VLC channel, they also propose an adaptive system with luminary selection and demonstrate improvements in spectral efficiency over non-adaptive systems.

In our work, the shadowing effect caused by the non-quantitative and randomly mobile obstructions (i.e., mobile users) with different characteristics such as size, position etc., is studied. In practice, especially for the mobile multi-users communication systems nowadays, the random shadowing is ubiquitous and has great effect on the performance of communication. Of course, on the condition that multiple LEDs are used in indoor VLC systems, it is impossible that all the optical links are blocked completely, namely, no absolute shadowing exists indoor. However, the shadowing can block some certain optical links and then partially attenuates the channel characteristics (i.e., received power) indeed, and it is important during channel characterization.

In this paper, the diffuse link is considered without loss of generality [18]. The Poisson process is introduced to describe the entrance of the moving objects into indoor VLC systems, and the probability density function is introduced to characterize the size and the position of the obstructions. In addition, a weighting function is proposed to describe shadowing effect. By utilizing mathematic statistics, a reasonable channel model for indoor VLC is set up. The expressions of the received power, the horizontal illuminance and the impulse responses are given. Through simulation, the proposed channel model turns out to be feasible, which can obtain channel impulse responses (CIRs) and RMS delay spread at any point in indoor VLC scenario. Based on the proposed channel model, the distributions of the received optical power and the signal-noise ratio (SNR) are obtained. And with comparison to the results presented by the conventional channel model for an empty room, the effect of random shadowing on communication performance is analyzed. On a deeper level, this paper analyzes the maximum available bandwidth in different communication environment with different numbers of randomly moving obstructions therein. A simulation optimization of the LEDs' direction and the photodetectors' field of view is also presented focusing on the SNR's coefficient of variation.

The remainder of the paper is organized as follows. In Section 2, we set up the channel model considering random shadowing. In Section 3, through simulation, we verify our model's feasibility of obtaining CIRs, as well as RMS delay spread, for any point indoor. In Section 4, based on the proposed channel model, we simulate and analyze the effect of random shadowing on communication performance. In Section 5, we conduct a simulation optimization for the indoor VLC system with random shadowing. We finally conclude in Section 6.

2. Channel Modeling

In this section, we model the indoor VLC channel to account for the shadowing resulting from the non-quantitative obstructions with random movement.

2.1 Statistical Methodology for Channel Modeling

The indoor topology can be arbitrary shape. For analysis, we assume that it is a cubic room ($X \times Y \times Z$). We assume that the number of the obstructions entering into the room obeys the Poisson process$N_t$with intensity parameter ε. Every obstruction has their own size (width w_i and height h_i) and position (x_i, y_i) independent and identically distributed. Whether each optical path is blocked or not can also be regarded as independent. In this case, a weighting function P_{AB} is presented to describe the probability of optical path AB being not blocked, where AB is a line segment connecting any two points A (x_A, y_A, z_A) and B (x_B, y_B, z_B). Fig. 1 is the schematic diagram, where some stationary articles are arranged in the room; L1, L2, L3 and L4 are LED lighting sources; the green area denotes one of the mobile obstructions whose thickness is neglected; and point G, whose coordinate is (x_v, y_v), is the midpoint of the projection of the mobile obstruction in the *x*-*y* plane.

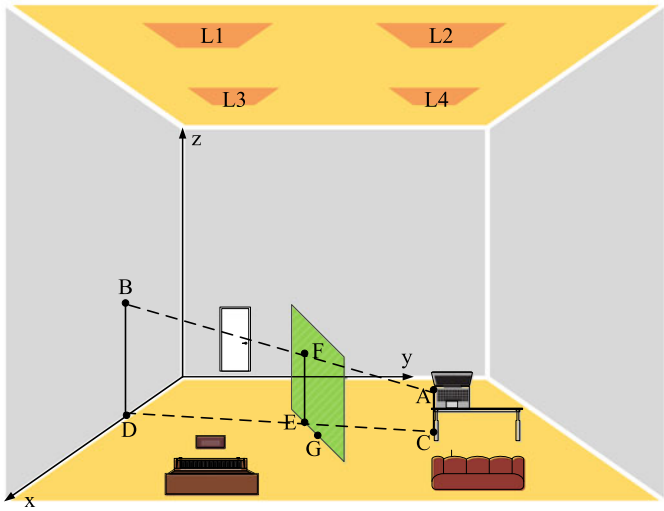

Fig. 1. Schematic diagram of optical path AB being blocked by a mobile obstruction with width w_v and height h_v in the indoor VLC system.

For the unshadowed case, the received power is given by the channel DC gain on directed path $H^{(0)}(0; S_i, R_j)$ and reflected path $H_{ref}(0; S_i, R_j)$ [19], [20]

$$P_r(R_j) = \sum_{i=1}^{I} [P_t H^{(0)}(0; S_i, R_j) + P_t H_{ref}(0; S_i, R_j)] \tag{1}$$

where, $P_r(R_j)$ is the received power of the receiver R_j, P_t is the transmitted power, I is the number of LEDs and S_i denotes the i-th LED. Due to multiple bounces, $H_{ref}(0; S_i, R_j)$ is expressed as follows [21]

$$H_{ref}(0; S_i, R_j) = \sum_{k=1}^{\infty} H^{(k)}(0; S_i, R_j) \tag{2}$$

where $H^{(k)}(0; S_i, R_j)$ is the channel DC gain after k bounces, which can be obtained by the recursive algorithm or the iterative algorithm.

For the shadowed case, a weighting function P_{AB}, mentioned above, is presented to describe the random shadowing deterministically. It is assumed that there is no obstruction in the room at the initial time. Moreover, the possible obstructions moving into the room within a period of t can be denoted by (w_1, h_1, x_1, y_1), (w_2, h_2, x_2, y_2), $\ldots$, $(w_{N_t}, h_{N_t}, x_{N_t}, y_{N_t})$. Let p_v denote the probability of optical path AB being blocked by (w_v, h_v, x_v, y_v), where v takes values from 1 to N_t.p_1, p_2, $\ldots$, p_{N_t} are all independent and identically distributed, hence P_{AB} can be described as

$$E\left[\prod_{v=1}^{N_t}(1 - p_v)\right] = \exp[-E(p_v)\varepsilon t] \tag{3}$$

(see Appendix A).

Let line segment CD represent the projection of line segment AB in the x-y plane, as shown in Fig. 1. Apparently, the coordinates of points C and D are $(x_A, y_A, 0)$, $(x_B, y_B, 0)$ respectively. Draw a line perpendicular to line CD from point (x_v, y_v) with point E being the foot point, and then construct a line EF parallel to z axis through point E, point F is the intersecting point with line AB. Now, the task now is to find out under what condition optical path AB will be blocked by (w_v, h_v, x_v, y_v). Considering the geometric relationships illustrated in Fig. 1, we can summarize the condition as follows:

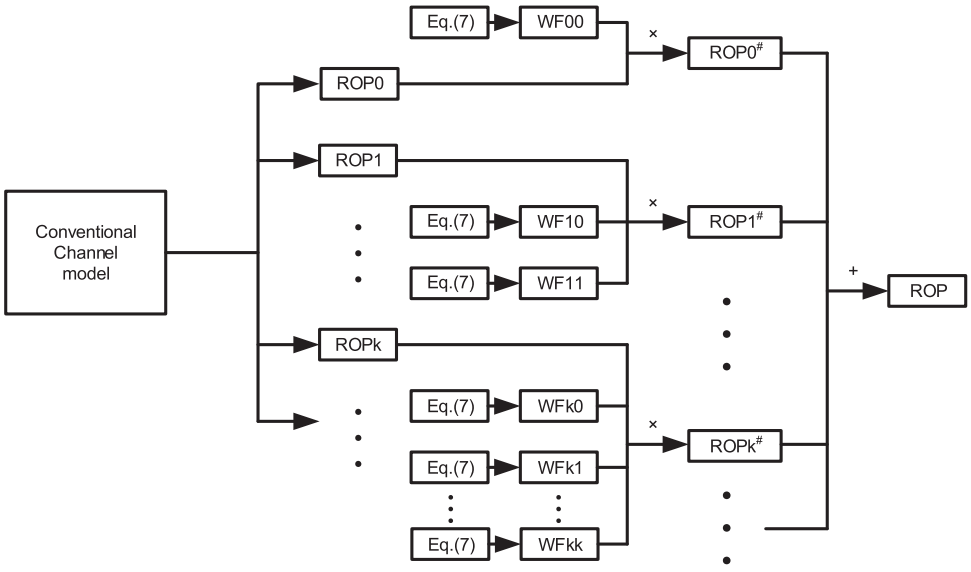

Fig. 2. Block diagram of the process of channel characterization.

(1) Half of w_v is greater than or equal to the distance of point (x_v, y_v) to line CD, namely,$w_v \geq 2d(x_v, y_v)$;
(2) h_v is greater than or equal to the length of line segment EF, namely, $h_v \geq s(x_v, y_v)$.

The coordinates of points A and B known, $d(x_v, y_v)$ and $s(x_v, y_v)$ can be calculated by utilizing the truths of geometry:

$$d(x_v, y_v) = \frac{\left|(y_A - y_B)x_v - (x_A - x_B)y_v - x_B y_A + x_A y_B\right|}{R_{AB} \sin\delta} \tag{4}$$

$$s(x_v, y_v) = \begin{cases} \frac{(R_{AB}\sin\delta)^2 + (x_v - x_B)^2 + (y_v - y_B)^2 - [(x_v - x_A)^2 + (y_v - y_A)^2]}{2R_{AB}\sin\delta} \cot\delta + z_B & z_B \leq z_A \\ \frac{(R_{AB}\sin\delta)^2 + (x_v - x_A)^2 + (y_v - y_A)^2 - [(x_v - x_B)^2 + (y_v - y_B)^2]}{2R_{AB}\sin\delta} \cot\delta + z_A & z_B > z_A \end{cases} \tag{5}$$

where, R_{AB} is the distance between points A and B, δ is the angle between line AB and z axis.

Let $g_v(w, h)$ denote the joint probability density function of w_v and h_v, as $f_v(x, y)$ does to x_v and y_v, the mathematic expectation of p_v, $E(p_v)$, can be calculated from the view of statistics:

$$E(p_v) = \int_0^X \int_0^Y \left(\iint_{\{(w,h):w \geq 2d(x,y), h \geq s(x,y)\}} g_v(w, h)dwdh \right) f_v(x, y)dxdy \tag{6}$$

(see Appendix B).

Combining with (3), P_{AB} can be obtained:

$$P_{AB} = \exp\left[-\varepsilon t \int_0^X \int_0^Y \left(\iint_{\{(w,h):w \geq 2d(x,y), h \geq s(x,y)\}} g_v(w, h)dwdh \right) f_v(x, y)dxdy \right] \tag{7}$$

2.2 Channel Characterization

Considering the generalized Lambertian radiation pattern of the transmitters and reflectors [19], [20] and multiplying the DC gain of each optical path by their corresponding weighting function respectively, we can determine a series of channel characteristics: the received optical power, the horizontal illuminance and the impulse responses. Fig. 2 illustrates our algorithm of channel characterization, wherein how the proposed random shadowing, namely weighting function P_{AB}, is used in channel modeling is shown in detail. In Fig. 2, ROP0, ROP1, and ROPk denote the

received optical power of the directed path, the first reflected path, and the k-th reflected path without random shadowing, respectively; while accounting for random shadowing, ROP0$^{\#}$, ROP1$^{\#}$, and ROPk$^{\#}$ denote the received optical power of the directed path, the first reflected path, and the k-th reflected path, respectively, and ROP denotes the total received optical power; WF00 denotes the weighting function of the directed path between LED and PD; for the first reflected path, WF10 and WF11 denote the weighting function of the path between LED and the reflection point, and between the first reflection point and PD, respectively; for the k-th reflected path, WFk0, WFk1, and WFkk denote the weighting function of the path between LED and the first reflection point, between the first reflection point and the second reflection point, and between the k-th reflection point and PD, respectively.

In addition, Fig. 2 takes the received optical power as example, the characterizations of horizontal Illuminance and impulse responses can be conducted in the same way.

2.2.1 Received Optical Power: Let $P_r(R_j)$ devote the received optical power at the point where the receiver R_j is located, then,

$$P_r(R_j) = \sum_{i=1}^{I} \left[P_t H^{(0)}(0; S_i, R_j) + P_t H_{ref}(0; S_i, R_j) \right] \tag{8}$$

$$H_{ref}(0; S_i, R_j) = \sum_{k=1}^{N} \int_{A_{sur}} H^{(k-1)}(0; S_i, dA_k) H^{(0)}(0; dA_k, R_j) \tag{9}$$

$$H^{(k-1)}(0; S_i, dA_k) = \int_{A_{sur}} H^{(k-2)}(0; S_i, dA_{k-1}) H^{(0)}(0; dA_{k-1}, dA_k) \tag{10}$$

$$H^{(0)}(0; S_i, R_j) = \frac{(m_s+1)A_{R_j}}{2\pi R_{S_i R_j}{}^2} \cos^{m_s}(\phi_{S_i R_j}) \cos(\varphi_{S_i R_j}) T_s(\varphi_{S_i R_j}) g(\varphi_{S_i R_j}) u(FOV_{R_j} - \varphi_{S_i R_j}) P_{S_i R_j} \tag{11}$$

$$H^{(0)}(0; S_i, dA_l) = \frac{(m_s+1)dA_l}{2\pi R_{S_i dA_l}{}^2} \cos^{m_s}(\phi_{S_i dA_l}) \cos(\varphi_{S_i dA_l}) u\left(\frac{\pi}{2} - \varphi_{S_i dA_l}\right) P_{S_i dA_l} \tag{12}$$

$$H^{(0)}(0; dA_f, dA_g) = \begin{cases} \frac{\rho_{dA_f}(m_e+1)dA_g}{2\pi R_{dA_f dA_g}{}^2} \cos^{m_e}(\phi_{dA_f dA_g}) \cos(\varphi_{dA_f dA_g}) u\left(\frac{\pi}{2} - \varphi_{dA_f dA_g}\right) P_{dA_f dA_g} & f \neq g \\ 0 & f = g \end{cases} \tag{13}$$

$$H^{(0)}(0; dA_n, R_j) = \frac{\rho_{dA_n}(m_e+1)A_{R_j}}{2\pi R_{dA_n R_j}{}^2} \cos^{m_e}(\phi_{dA_n R_j}) \cos(\varphi_{dA_n R_j}) \times T_s(\varphi_{dA_n R_j}) g(\varphi_{dA_n R_j}) u(FOV_{R_j} - \varphi_{dA_n R_j}) P_{dA_n R_j} \tag{14}$$

where, dA_k, $dA_{k-1}, \ldots, dA_1$ devote the area of the independent differential reflecting element respectively [3]–[8] and the integration is performed with respect to the surface A_{sur} of all reflectors; the variables whose subscripts are $S_i dA_l$ are defined for the two points that correspond to the i-th light source and the differential element dA_l approximately; likewise, the variables whose subscripts are $dA_f dA_g$, $dA_n R_j$ or $S_i R_j$ are defined; N is the number of bounces considered; A_{R_j} is the physical area of the detector in the receiver R_j; R is the distance between the corresponding two points; ϕ is the angle of irradiance; φ is the angle of incidence; m is the directivity of an emission pattern, which is derived from a semiangle at half power $\Phi_{1/2}$, $m = -\ln 2 / \ln \cos \Phi_{1/2}$; m_s and m_e are for the light sources and the reflectors respectively; $u(\cdot)$ is an step function; FOV_{R_j} is the width of the field of view at the receiver R_j; P denotes the proposed weighting function; ρ_{dA_f} and ρ_{dA_n} are the reflectance values of the differential reflecting element dA_f and dA_n respectively; $T_s(\varphi)$ is the gain of an optical filter and $g(\varphi)$ is the gain of an optical concentrator which is given as [22]

$$g(\varphi) = \begin{cases} \frac{n^2}{\sin^2 FOV_{R_j}} & 0 \leq \varphi \leq FOV_{R_j} \\ 0 & \varphi \geq FOV_{R_j} \end{cases} \tag{15}$$

where n denotes the refractive index.

2.2.2 Horizontal Illuminance: In the same way, the horizontal illuminance [19]–[21] at any point where the receiver R_j is located, $E_{hor}(R_j)$, can be obtained.

$$E_{hor}(R_j) = \sum_{i=1}^{I} [E^{(0)}(S_i, R_j) + E_{ref}(S_i, R_j)] \tag{16}$$

$$E_{ref}(S_i, R_j) = \sum_{k=1}^{N} \int_{A_{sur}} E^{(k-1)}(S_i, dA_k) E^{(0)}(dA_k, R_j) \tag{17}$$

$$E^{(k-1)}(S_i, dA_k) = \int_{A_{sur}} E^{(k-2)}(S_i, dA_{k-1}) E^{(0)}(dA_{k-1}, dA_k) \tag{18}$$

$$E^{(0)}(S_i, R_j) = \frac{I(0)}{{R_{S_iR_j}}^2} \cos^{m_s}(\phi_{S_iR_j}) \cos(\varphi_{S_iR_j}) P_{S_iR_j} \tag{19}$$

$$E^{(0)}(S_i, dA_l) = \frac{I(0)}{{R_{S_idA_l}}^2} \cos^{m_s}(\phi_{S_idA_l}) \cos(\varphi_{S_idA_l}) P_{S_idA_l} \tag{20}$$

$$E^{(0)}(dA_f, dA_g) = \begin{cases} \frac{(m_e+1)\rho_{dA_f}}{2\pi {R_{dA_fdA_g}}^2} \cos^{m_e}(\phi_{dA_fdA_g}) \cos(\varphi_{dA_fdA_g}) P_{dA_fdA_g} & f \neq g \\ 0 & f = g \end{cases} \tag{21}$$

$$E^{(0)}(dA_n, R_j) = \frac{(m_e+1)\rho_{dA_n}}{2\pi {R_{dA_nR_j}}^2} \cos^{m_e}(\phi_{dA_nR_j}) \cos(\varphi_{dA_nR_j}) P_{dA_nR_j} \tag{22}$$

where, $I(0)$ is the center luminous intensity of an LED and m_e is usually set as 1.

2.2.3 Impulse Responses: The impulse responses [3]–[17] between the transmitter S_i and the receiver R_j accounting for random shadowing, $h(t; S_i, R_j)$, can be also determined.

$$h(t; S_i, R_j) = \sum_{k=0}^{N} h^{(k)}(t; S_i, R_j) \tag{23}$$

$$h^{(k)}(t; S_i, R_j) = \int_{A_{sur}} h^{(k-1)}(t; S_i, dA_k) \otimes h^{(0)}(t; dA_k, R_j) \tag{24}$$

$$h^{(0)}(t; S_i, R_j) = \frac{(m_s+1)A_{R_j}}{2\pi {R_{S_iR_j}}^2} \cos^{m_s}(\phi_{S_iR_j}) \cos(\varphi_{S_iR_j}) T_s(\varphi_{S_iR_j}) \times g(\varphi_{S_iR_j}) u(FOV_{R_j} - \varphi_{S_iR_j}) \delta\left(t - \frac{R_{S_iR_j}}{c}\right) P_{S_iR_j} \tag{25}$$

$$h^{(0)}(t; S_i, dA_l) = \frac{(m_s+1)dA_l}{2\pi {R_{S_idA_l}}^2} \cos^{m_s}(\phi_{S_idA_l}) \cos(\varphi_{S_idA_l}) u\left(\frac{\pi}{2} - \varphi_{S_idA_l}\right) \delta\left(t - \frac{R_{S_idA_l}}{c}\right) P_{S_idA_l} \tag{26}$$

$$h^{(0)}(t; dA_f, dA_g) = \begin{cases} \frac{\rho_{dA_f}(m_e+1)dA_g}{2\pi {R_{dA_fdA_g}}^2} \cos^{m_e}(\phi_{dA_fdA_g}) \cos(\varphi_{dA_fdA_g}) & \\ \times u(\frac{\pi}{2} - \varphi_{dA_fdA_g}) \delta(t - \frac{R_{dA_fdA_g}}{c}) P_{dA_fdA_g} & f \neq g \\ 0 & f = g \end{cases} \tag{27}$$

$$h^{(0)}(t; dA_n, R_j) = \frac{\rho_{dA_n}(m_e+1)A_{R_j}}{2\pi {R_{dA_nR_j}}^2} \cos^{m_e}(\phi_{dA_nR_j}) \cos(\varphi_{dA_nR_j}) T_s(\varphi_{dA_nR_j}) \times g(\varphi_{dA_nR_j}) u(FOV_{R_j} - \varphi_{dA_nR_j}) \delta\left(t - \frac{R_{dA_nR_j}}{c}\right) P_{dA_nR_j} \tag{28}$$

where, c denotes the speed of light, m_e is usually set as 1, $\otimes$ means convolution.

It's worth noting that we consider flexible reflectance values for different surface materials (i.e., plaster wall, plastic wall, floor, ceiling, etc), ρ_{dA_f} and ρ_{dA_n} in the above formulas prove the behavior.

In addition, our model can be easily extended to take the wavelength dependency of reflectance into account. Let λ denote wavelength, the power spectral distribution (PSD) of phosphor-based white LEDs, $\Phi(\lambda)$, and spectral reflectance of various materials in the visible light bandwidth are illustrated in [4] (seen in Fig. 1). Under the premise, $\Gamma_n^{(k)}$, which denotes the power of the reflected ray after *k*-bounces from the *n*-th LED, can be exactly calculated as [4]

$$\Gamma_n^{(k)} = \int_\lambda \Phi_n(\lambda)\rho_1(\lambda)\rho_2(\lambda)\cdots\rho_k(\lambda)d\lambda \tag{29}$$

The simplified form with lower accuracy can be described by [4]

$$\bar{\Gamma}_n^{(k)} = P_n\bar{\rho}_{n,1}\bar{\rho}_{n,2}\cdots\bar{\rho}_{n,k} \tag{30}$$

where, $\bar{\rho}_{n,k} = \frac{1}{P_n}\int_\lambda \Phi_n(\lambda)\rho_k(\lambda)d\lambda$ is the average reflectance, and $P_n = \int_\lambda \Phi_n(\lambda)d\lambda$ is the radiant power of the *n*-th LED. Hence, what's needed in our model is to adopt $\bar{\rho}_{dA_f}$ and $\bar{\rho}_{dA_n}$, instead of ρ_{dA_f} and ρ_{dA_n}.

3. Numerical Model Simulation

In this section, we simulate the CIRs and RMS delay spread based on the proposed channel model. A 5 m $\times$ 5m $\times$ 3 m room is chosen. Five scenarios are simulated for examples: scenario 1, an empty room; scenario 2, a room where mobile obstructions entering at a Poisson process with intensity parameter ε being 5 per minute; scenario 3, a room where mobile obstructions entering at a Poisson process with intensity parameter ε being 10 per minute; scenario 4, a room where mobile obstructions entering at a Poisson process with intensity parameter ε being 20 per minute; scenario 5, a room where a stationary cuboid obstruction being located and mobile obstructions entering at a Poisson process with intensity parameter ε being 10 per minute. Besides, we assume that the duration of the Poisson entry is 5min. Other system parameters are listed in Table 1.

It's worth noting that the joint probability density function $g_v(w, h)$ and $f_v(x, y)$ can be arbitrary, which depends on the actual situation. For illustrative purposes, we consider the uniform distribution. Likewise, if we assign other functions to $g_v(w, h)$ and $f_v(x, y)$ according to the actual situation, we only need to substitute them into the equations in our model correspondingly.

3.1 Channel Impulse Responses

Fig. 3 shows the channel impulse responses for all the scenarios. According to Fig. 2, it's easy to find that when the weighting functions of all optical links are equal to 1, our channel model corresponds to the conventional model. For scenario 1, namely an empty room, we calculate the weighting functions of all optical links by (7) and the results are all equal to 1. Apparently, our channel model is compatible with the conventional one.

From the above figures, the effect of random shadowing is shown by comparing Fig. 3(b)–(d) with Fig. 3(a); wherein Fig. 3(b)–(d) present the trend of random shadowing with the increase in intensity parameter ε. In addition, under the condition of the same random shadowing effect, we show the effect of the stationary obstruction by comparing Fig. 3(e) with (c).

The peak of the blue curve for one-bounce CIRs is about 97W/s, 42 W/s, 18 W/s and 4 W/s for Fig. 3(a)–(d), respectively; likewise, the peak of the red curve for two-bounce CIRs is about 10 W/s, 6 W/s, 4 W/s and 2 W/s for Fig. 3(a)–(d), respectively. It can be seen that the existence of randomly mobile obstructions significantly decreases the CIRs. With the increase in intensity parameter ε, the random shadowing effect becomes more and more serious and the CIRs get smaller and smaller, as shown in Fig. 3(b)–(d). Comparing Fig. 3(e) with (c), we can find that the existence of the stationary obstruction induces one more peak for one-bounce CIRs when time delay is around 13 ns. This is because that the stationary obstruction surface serves as the reflective surface for the first bounce. The amplitude of the new peak is around 6 times larger than that of the peak of one-bounce CIRs without the stationary obstruction. The reason is as follows: when the stationary obstruction surface serves for the first bounce, the optical link has a smaller transmission distance, as well as the angle

TABLE 1
System parameters

Materials of the room surface (north, south, west, east, ceiling, floor)	(Aluminum, Aluminum, Plate Window Glass, Pine Wood, Plaster, Black Gloss Paint)
Number of LED	1
Transmitted power (blue component) of the LED	1 W
LED's semi-angle at half power	60°
LED position (m)	(2.5, 2.5, 3)
Elevation and azimuth of the LED	90°, 0°
Physical area of PD	1 (cm^2)
FOV (Field of View) of PD	70°
Responsivity of PD (Si-APD)	0.53 A/W
PD position (m)	(2.5, 2.5, 0)
Elevation and azimuth of PD	90°,0°
Gain of the optical filter	1
Gain of the optical concentrator	1
Vertexes coordinates of the stationary obstruction (m)	(3.65, 0, 0), (3.85, 0, 0), (3.65, 10/3, 0), (3.85, 10/3, 0), (3.65, 0, 2), (3.85, 0, 2), (3.65, 10/3, 2), (3.85, 10/3, 2)
Materials of the stationary obstruction surface (north, south, west, east, top, bottom)	(Plaster, Plaster, Light-absorbing material, Light-absorbing material, Light-absorbing material, Light-absorbing material)
Materials of mobile user surface (north, south, west, east, top, bottom)	(Light-absorbing material, Light-absorbing material, Light-absorbing material, Light-absorbing material, Light-absorbing material, Light-absorbing material)
$g_v(w, h)$	$U(0, 2)$
$f_v(x, y)$	$U(0, 25)$
Time resolution	0.5 (ns)
Space resolution	0.25 (m)

of irradiance, thus providing a higher channel DC gain; in addition, the reflectance of the room surface (around 0.58) is smaller than that of the stationary obstruction surface (around 0.8) in our simulation. The multiple is around 6 occasionally in our simulation scenario and it varies if the simulation scenario differs (i.e., different positions or sizes of the stationary obstruction, different reflectances, etc.). Moreover, the stationary obstruction has little effect on two-bounce CIRs. The reason is that a single reflective surface takes up a smaller and smaller proportion with the increase in the order of reflection.

3.2 Time Dispersion

Once we obtain CIRs, we can calculate the time dispersion parameters of channel such as RMS delay spread and mean excess delay, which are, respectively, given by [18]

$$\tau_{RMS} = \sqrt{\frac{\int_{-\infty}^{\infty} (t - \tau_0)^2 h^2(t) dt}{\int_{-\infty}^{\infty} h^2(t) dt}} \tag{31}$$

$$\tau_0 = \frac{\int_{-\infty}^{\infty} t h^2(t) dt}{\int_{-\infty}^{\infty} h^2(t) dt} \tag{32}$$

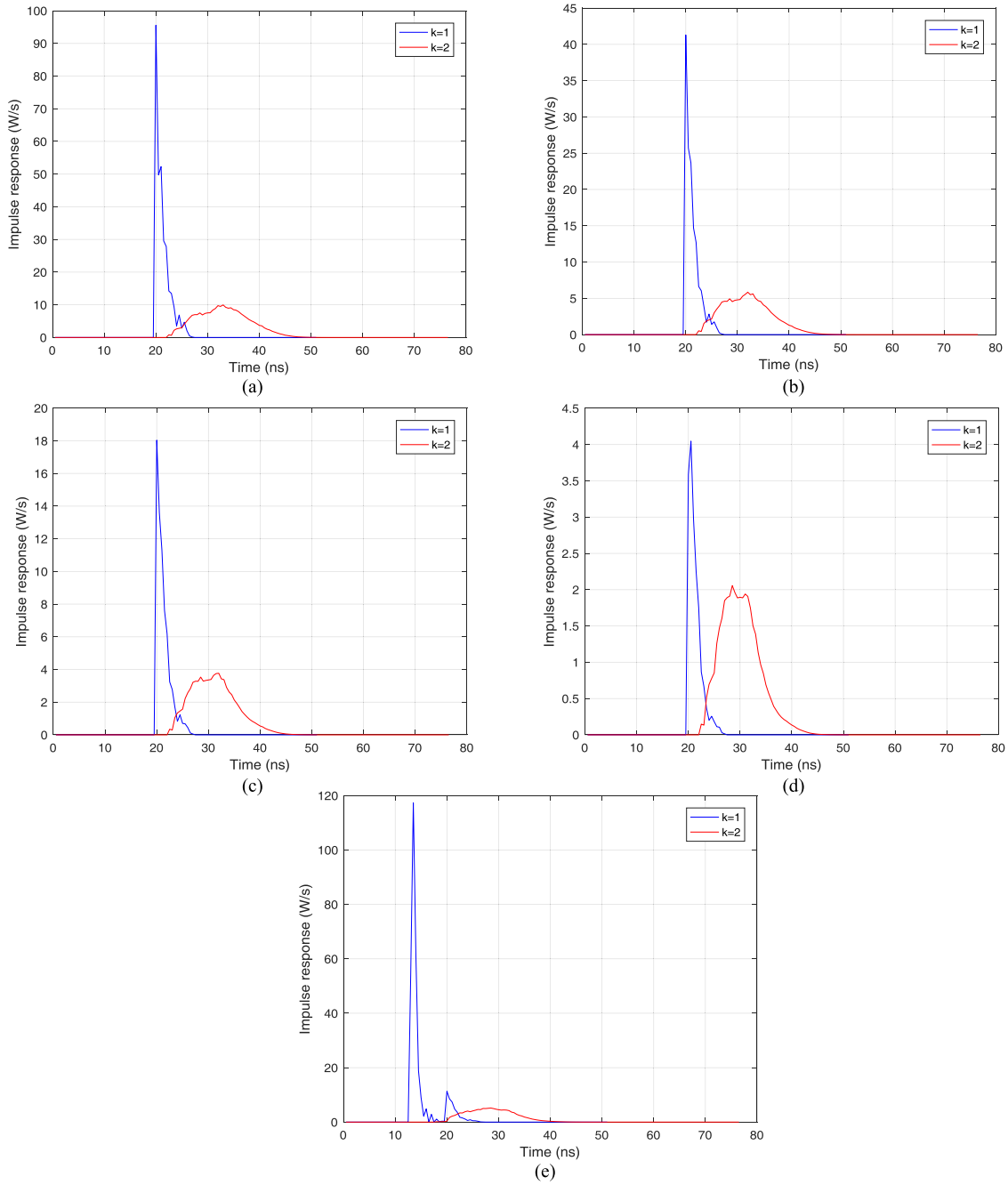

Fig. 3. Channel impulse responses at the PD's position in (a) scenario 1; (b) scenario 2; (c) scenario 3; (d) scenario 4; (e) scenario 5, where *k* corresponds to the *k*-th bounce.

Concerning the above scenarios, the time dispersion parameters of channel at the PD's position are shown in Table 2.

We can conclude from Table 2 that the existence of randomly mobile obstructions decreases both mean excess delay and RMS delay spread. Differently, the existence of the stationary obstruction decreases mean excess delay while increases RMS delay spread. The reason is as follows. First, while the stationary obstruction surface serves as the reflective surface for some certain optical links, the corresponding time delays are lower than those with the room walls as the reflective surface,

TABLE 2
Mean Excess Delay and RMS Delay Spread for Different Scenarios

	τ_0(ns)	τ_{RMS}(ns)
Scenario 1	12.29	4.99
Scenario 2	10.65	3.27
Scenario 3	10.61	2.44
Scenario 4	10.57	1.54
Scenario 5	10.24	3.16

hence mean excess delay decreases overall. Then, concerning the same order of reflection, the time delays of all the optical links are almost the same to a certain extent without the stationary obstruction wherein, however, the existence of the stationary obstruction greatly decreases the time delays of some certain optical links as mentioned above, which leads to a larger variance, as a result, RMS delay spread increases.

It should be emphasized that we assume an LED and a fixed PD's position just for verification of the proposed model's feasibility. In reality, distributed LED array lighting sources composed of many LEDs are often utilized for communication concurrent with illumination. We only need to superpose all the solutions induced by each LED, which will be involved in the next section for 4 LEDs. Apparently, no matter where the PD is located, the new model can work in the same way.

4. Communication Performance Simulation and Analysis

As is well known, the performance of a communication system is evaluated by reliability (SNR or BER) and validity (channel bandwidth). Therefore, in this section, based on our model, we conduct a simulation and analysis of communication performance of a VLC system involving random shadowing.

In order to be more practical, we make some improvements to the system parameters set in Section 3. We adopt 4 LED lighting sources and each of them has a TX power of 15 W. The coordinates of these lighting sources are (1.5, 1.5, 3), (1.5, 3.5, 3), (3.5, 1.5, 3) and (3.5, 3.5, 3), respectively. The other system parameters are the same as the above.

4.1 SNR

In the VLC, the SNR can be calculated by [23]

$$SNR = \frac{\gamma^2 K^2 P_r^2}{2e\gamma(P_r + P_b + P_{ISI})B + 2eI_d B + \sigma^2_{thermal} + \gamma^2 P^2_{ISI}} \approx \frac{\gamma K^2 P_r}{2eB} \tag{33}$$

where, γ denotes the responsivity of PD, K means the ratio of signal power to total power, P_r is the received optical power, e denotes the electronic charge, P_b denotes the background noise, P_{ISI} denotes the inter-symbol interference noise, B denotes bandwidth, I_d is the dark current and $\sigma^2_{thermal}$ means the thermal noise variance.

Once the SNR is known, the BER can be correspondingly obtained according to the modulation scheme. Take NRZ-OOK for example, the relationship between SNR and BER can be expressed as

$$BER = Q(\sqrt{SNR}) \tag{34}$$

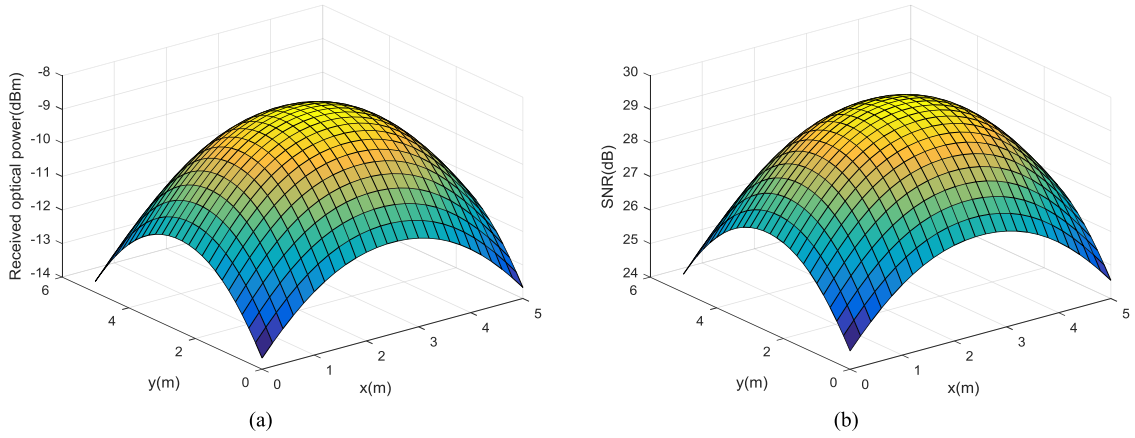

Fig. 4. The distribution of (a) received optical power, Min. -13.67dBm, Max. -8.48 dBm, Ave. -10.38 dBm and (b) SNR, Min. 24.54 dB, Max. 29.73 dB, Ave. 27.83 dB in scenario 1.

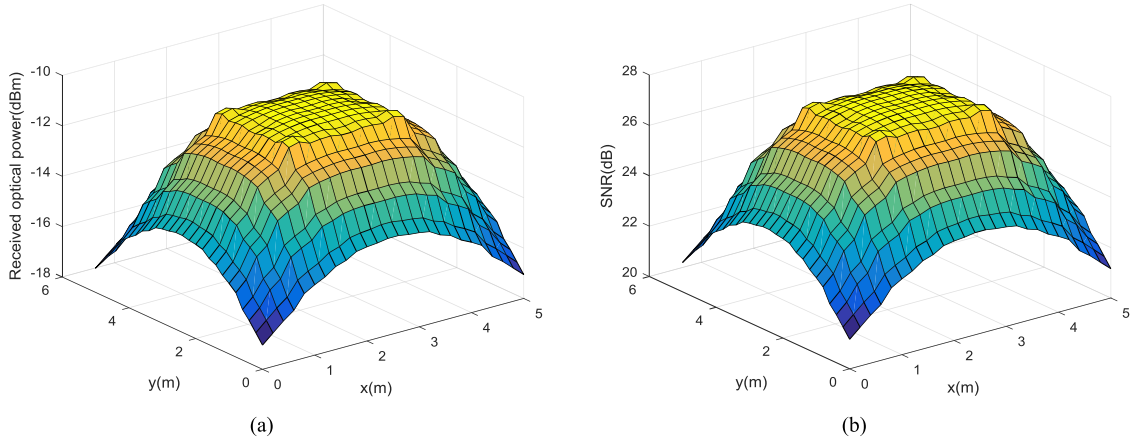

Fig. 5. The distribution of (a) received optical power, Min. −17.05 dBm, Max. −10.54 dBm, Ave. −12.83 dBm and (b) SNR, Min. 21.16 dB, Max. 27.68 dB, Ave. 25.38 dB in scenario 3.

where $Q(\cdot)$ is Q-function. Apparently, in order to guarantee the BER below 1×10^{-6}, the SNR must be greater than 13.6 dB.

We choose $B = 100$ MHz, $K = 0.02$ and simulation step $\Delta l = 0.2$ m, then, the distribution of received optical power and SNR is shown in Figs. 4–6 for scenario 1, scenario 3 and scenario 5 respectively.

Comparing Fig. 5 with Fig. 4, we can find that the existence of randomly mobile obstructions in scenario 3 decreases the average SNR by ∼2.5 dB and makes the distribution of received optical power, as well as SNR, not smooth any more. However, SNR on the entire receiving plane is higher than the threshold of 13.6 dB [19], which means the indoor VLC system is still reliable while the bandwidth is 100 MHz. Besides, it can be seen from Fig. 6 that the existence of the stationary obstruction may cause outage of illumination and communication at some certain receiving points. The corresponding solution is to install additional LEDs around the stationary obstruction based on the actual situation.

4.2 Channel Bandwidth

We explore the maximum available bandwidths in scenario 1, 2, 3 and 4 respectively under the constraint condition that the minimum SNR on the entire receiving plane is higher than the threshold of 13.6 dB [19]. According to preceding text, in scenario 5, it makes no sense to discuss the minimum

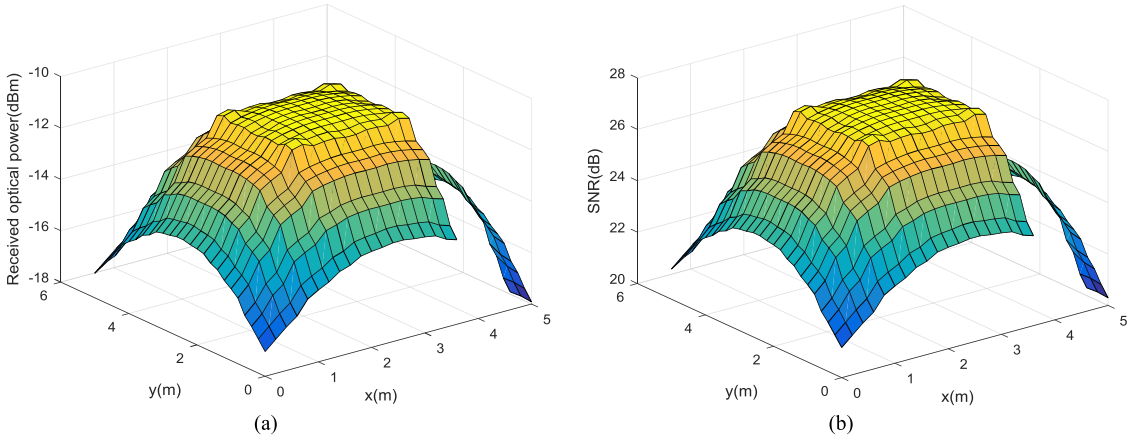

Fig. 6. The distribution of (a) received optical power, Min. -Inf, Max. −10.54 dBm, Ave. -Inf and (b) SNR, Min. -Inf, Max. 27.68 dB, Ave. -Inf in scenario 5.

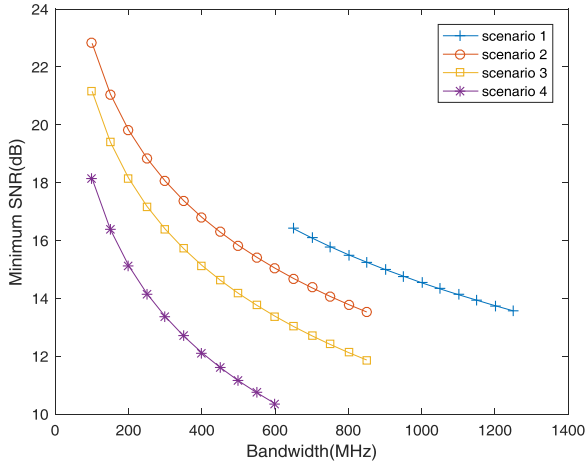

Fig. 7. The minimum SNR variations of different bandwidths in different environment.

SNR due to the outage. Therefore, a simulation is conducted for scenario 1, 2, 3 and 4 to show the minimum SNR variations of different bandwidths, as illustrated in Fig. 7.

With the minimum SNR of 13.6 dB as the constraint condition, we can conclude from Fig. 7 that the maximum available bandwidths in scenario 1, 2, 3 and 4 are 1200 MHz, 800 MHz, 550 MHz and 250 MHz, respectively. The reason for the divergence lies in different numbers of randomly moving obstructions therein, namely, with the increase of the randomly moving obstructions, the available bandwidth will decrease.

However, the modulation bandwidth of LED is limited due to its low-pass filter nature. Currently, the modulation bandwidth reaches only 175 MHz [24] for WLED utilizing blue filter, equalization technique, and pre-emphasis technique. Taking the modulation bandwidth into consideration, we can conclude that the available bandwidths in the four scenarios are all equal to 175 MHz. Moreover, it can be foreseen that if more randomly moving obstructions exist, the available bandwidth can be less than the modulation bandwidth.

5. Simulation Optimization

In this Section, in terms of the LEDs' direction and the PD's FOV, we conduct a simulation optimization for the randomly shadowing VLC system.

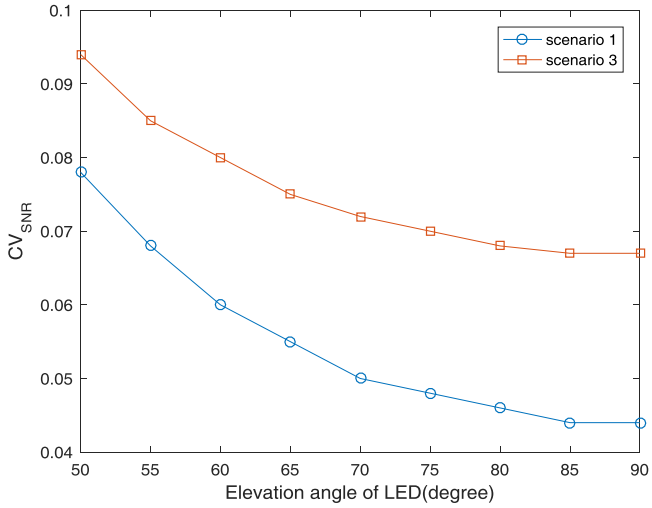

Fig. 8. CV_{SNR} variations of different elevation angles of LED in different environment.

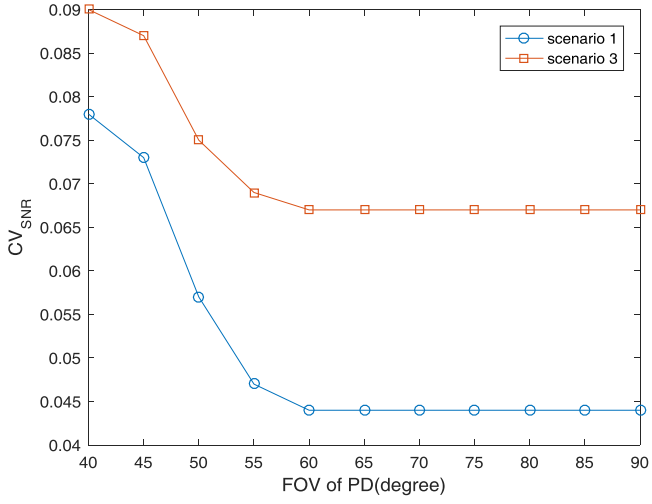

Fig. 9. CV_{SNR} variations of different FOVs of PD in different environment.

It should be noted that our simulation optimization aims to acquire a high level of average SNR and low dispersion of SNR which means the variability in the level of SNR at different positions in the room. Because the average SNR is always small while the variance of SNR is small, the dispersion of SNR should not be measured by the variance, but the coefficient of variation CV_{SNR}, which is defined as the ratio between the standard deviation of SNR to the mean SNR [25]

$$CV_{SNR} = \sigma_{SNR}/\mu_{SNR} \tag{35}$$

5.1 Elevation Angle of LED

First we choose a set of common values for the elevation angle of LED; then based on our channel model, we calculate the coefficient of variation CV_{SNR} for each elevation angle value using MATLAB; finally we select the elevation angle value, which corresponds to the minimum CV_{SNR}, as the optimal one. Fig. 8 shows CV_{SNR} variations of different elevation angles of LED in scenario 1 and scenario 3.

It can be seen from Fig. 8 that the existence of randomly mobile obstructions leads to greater CV_{SNR}, which is consistent with preceding presentation concerning the unsmooth distribution of SNR. Moreover, no matter whether randomly mobile obstructions exist or not, the optimal elevation angle of LED should be 90°.

5.2 FOV of PD

The optimization approach is the same as that for the elevation angle of LED. Fig. 9 shows CV_{SNR} variations of different FOVs of PD in scenario 1 and scenario 3.

It's worth noting that CV_{SNR} is not a number while PD's FOV is smaller than 40°, which means the existence of outage at some certain receiving points no matter whether randomly mobile obstructions exist or not. Moreover, CV_{SNR} reaches the minimum value while PD's FOV is larger than 60°. In general, larger PD's FOV means louder noise, hence the optimal FOV of PD should be 60°.

6. Conclusion

In this paper, considering the effect of the random shadowing induced by the non-quantitative and randomly mobile obstructions, we study the channel characteristics of indoor VLC systems. In our discussion, the entrance of the moving objects obeys the Poisson process, and the size and position of the obstructions are described by the probability density function. In addition, a weighting function is statistically presented to account for the random shadowing. On this basis, a reasonable channel model is set up. The expressions of the received power, the horizontal illuminance and the impulse response are given. We verify the new model's feasibility of obtaining CIRs and RMS delay spread. On a deeper level, the effect of random shadowing on communication performance is analyzed and a simulation optimization is conducted based on the new model. What's gratifying is that our channel model is general in use regardless of the positions of the light sources and the receivers (i.e., on the ceiling, walls, desk, etc.). Apparently, the model is able to be applied to uplink or downlink, and the key issue is to compare z_A andz_B in (5).

The proposed model is based on the conventional channel model and shows complete compatibility. It's worth noting that our method to deal with "random shadowing" can be adopted in other VLC channel models such as the reference model of 802.15.7r1. We only need to multiply the obtained channel DC gain of any optical link by its corresponding weight, which can accord with indoor VLC channel better, especially for multi-users mobile VLC systems.

Appendix A

$$
\begin{aligned}
&E\left[\prod_{v=1}^{N_t}(1-p_v)\right] \\
&= E\left[\prod_{v=1}^{N_t}(1-p_v)\right] \\
&= E\left\{E\left[\prod_{v=1}^{N_t}(1-p_v)\middle| N_t\right]\right\} \\
&= E[f(N_t)]
\end{aligned}
$$

$$
\begin{aligned}
&= \sum_{k=0}^{\infty} f(k) P(N_t = k) \\
&= \sum_{k=0}^{\infty} \left\{ E\left[\prod_{v=1}^{k} (1 - p_v) \right] \right\} \frac{(\varepsilon t)^k \exp(-\varepsilon t)}{k!} \\
&= \sum_{k=0}^{\infty} \left[\prod_{v=1}^{k} E(1 - p_v) \right] \frac{(\varepsilon t)^k \exp(-\varepsilon t)}{k!} \\
&= \sum_{k=0}^{\infty} \left\{ \prod_{v=1}^{k} [1 - E(p_v)] \right\} \frac{(\varepsilon t)^k \exp(-\varepsilon t)}{k!} \\
&= \sum_{k=0}^{\infty} [1 - E(p_v)]^k \frac{(\varepsilon t)^k \exp(-\varepsilon t)}{k!} \\
&= \exp(-\varepsilon t) \sum_{k=0}^{\infty} \frac{\{[1 - E(p_v)]\varepsilon t\}^k}{k!} \\
&= \exp(-\varepsilon t) \exp[(1 - E(p_v))\varepsilon t] \\
&= \exp\left[-\varepsilon E(p_v) t\right]
\end{aligned}
$$

Appendix B

$$
\begin{aligned}
&E(p_v) \\
&= E\left[E(p_v | x_v, y_v)\right] \\
&= E\left\{E\left[\Re_{\{w_v \geq 2d(x_v, y_v), h_v \geq s(x_v, y_v)\}}\right]\right\} \\
&= E\left[\iint \Re_{\{w \geq 2d(x_v, y_v), h \geq s(x_v, y_v)\}} g_v(w, h) dw dh\right] \\
&= E\left[\iint_{\{(w,h): w \geq 2d(x_v, y_v), h \geq s(x_v, y_v)\}} g_v(w, h) dw dh\right] \\
&= \iint_{\{(x,y): x \in [0, X], y \in [0, Y]\}} \left(\iint_{\{(w,h): w \geq 2d(x,y), h \geq s(x,y)\}} g_v(w, h) dw dh \right) f_v(x, y) dx dy \\
&= \int_0^X \int_0^Y \left(\iint_{\{(w,h): w \geq 2d(x,y), h \geq s(x,y)\}} g_v(w, h) dw dh \right) f_v(x, y) dx dy
\end{aligned}
$$

References

[1] T. Shang, T. Jiang, Y. Yang, P. Wang, and Y. Liu, "Multi-users network model and the corresponding networking scheme for indoor VLC systems," *Opt. Exp.*, vol. 23, no. 9, pp. 11600–18, 2015.

[2] Y. Wang, J. Shi, C. Yang, Y. Wang, and N. Chi, "Integrated 10 Gb/s multilevel multiband passive optical network and 500 Mb/s indoor visible light communication system based on Nyquist single carrier frequency domain equalization modulation," *Opt. Lett.*, vol. 39, no. 9, pp. 2576–2579, 2014.

[3] K. Lee, and H. Park, "Channel model and modulation schemes for visible light communications," in *Proc. IEEE 54th Int. Midwest Symp. Circuits Syst.*, 2011, pp. 1–4.

[4] K. Lee, H. Park, and J. R. Barry, "Indoor channel characteristics for visible light communications," *Commun. Lett.*, vol. 15, no. 2, pp. 217–219, 2011.

[5] H. Chun, C. J. Chiang, and D. C. O'Brien, "Visible light communication using OLEDs: Illumination and channel modeling," in *Proc. IEEE Int. Workshop Opt. Wireless Commun.*, 2012, pp. 1–3.
[6] X. Zhang, K. Cui, M. Yao, and H. Zhang, "Experimental characterization of indoor visible light communication channels," in *Proc. IEEE Int. Symp. Commun. Syst., Netw. Digital Signal Process.*, 2012, pp. 1–5.
[7] S. Long, M. A. Khalighi, M. Wolf, and S. Bourennane, "Channel characterization for indoor visible light communications," in *Proc. IEEE 3rd Int. Workshop Opt. Wireless Commun.*, 2014, pp. 75–79.
[8] J. Ding, and Z. Xu, "Performance of Indoor VLC and Illumination under Multiple Reflections," in *Proc. 6th Int. Conf. Wireless Commun. Signal Process.*, 2014, pp. 1–6.
[9] Y. Xiang, M. Zhang, M. Kavehrad, M. I. S. Chowdhury, M. Liu, J. Wu, and X. Tang, "Human shadowing effect on indoor visible light communications channel characteristics," *Opt. Eng.*, vol. 53, no. 8, 2014, Art. no. 086113.
[10] M. Farshad and M. Uysal, "Channel modeling and characterization for visible light communications," *IEEE Photon. J.*, vol. 7, no. 6, Dec. 2015, Art. no. 7905616.
[11] F. Miramirkhani, O. Narmanlioglu, M. Uysal, and E. Panayirci, "A mobile channel model for VLC and application to adaptive system design," *IEEE Commun. Lett.*, vol. 21, no. 5, pp. 1035–1038, May 2017.
[12] M. Uysal, F. Miramirkhani, O. Narmanlioglu, T. Baykas, and E. Panayirci, "IEEE 802.15.7r1 reference channel models for visible light communications," *IEEE Commun. Mag.*, vol. 55, no. 1, pp. 212–217, Jan. 2017.
[13] J. R. Barry, and J. M. Khan, "Simulation of multipath impulse response for indoor wireless optical channels," *IEEE J. Sel. Areas Commun.*, vol. 11, no. 3, pp. 367–379, Apr. 1993.
[14] R. Perez-Jimenez, J. Berges, and M. J. Betancor, "Statistical model for the impulse response on the infrared indoor diffuse channels," *Electron. Lett.*, vol. 33, no. 15, pp. 1298–1301, 1997.
[15] F. J. Lopez-Hernandez, and M. J. Betancor, "DUSTIN: algorithm for calculation of impulse response on IR wireless indoor channels," *Electron. Lett.*, vol. 33, no. 21, pp. 1804–1806, 1997.
[16] R. Perez-Jimenez, F. J. Lopez-Hernandez, and A. Santamaria, "Modified Monte Carlo scheme for high-efficiency simulation of the impulse response on diffuse IR wireless indoor channels," *Electron. Lett.*, vol. 34, no. 19, pp. 1819–1820, 1998.
[17] J. B. Carruthers, and P. Kannan, "Iterative site-based modeling for wireless infrared channels," *IEEE Trans. Antennas Propag.*, vol. 50, no. 5, pp. 759–765, May 2002.
[18] J. M. Kahn, and J. R. Barry, "Wireless infrared communications," *Proc. IEEE*, vol. 85, no. 2, pp. 265–298, 1997.
[19] T. Komine, and M. Nakagawa, "Fundamental analysis for visible light communication system using LED lights," *IEEE Trans. Consum. Electr.*, vol. 50, no. 1, pp. 100–107, Feb. 2004.
[20] J. Grubor, S. Randel, K. D. Langer, and J. W. Walewski, "Broadband information broadcasting using LED-based interior lighting," *J. Lightw. Technol.*, vol. 26, no. 24, pp. 3883–3892, Dec. 2008.
[21] J. R. Barry, J. M. Kahn, W. J. Krause, E. A. Lee, and D. G. Messerschmitt, "Simulation of multipath impulse response for indoor wireless optical channels," *IEEE J. Sel. Area Comm.*, vol. 11, no. 3, pp. 367–379, Sep. 2006.
[22] J. R. Barry, *Wireless Infrared Communications*, Norwell, MA, USA: Kluwer, 1994.
[23] T. Chen, L. Liu, and W. Hu, "Capacity analysis for indoor visible light communication systems," in *Proc. Asia Commun. Photon. Conf.*, 2013, Paper AF2F.23.
[24] H. Li, X. Chen, J. Guo, Z. Gao, and H. Chen, "An analog modulator for 460 Mb/s visible light data transmission based on OOK-NRS modulation," *IEEE Wireless Commun.*, vol. 22, no. 2, pp. 68–73, Apr. 2015.
[25] D. Tronghop, J. Hwang, S. Jung, Y. Shin, and M. Yoo, "Modeling and analysis of the wireless channel formed by LED angle in visible light communication," in *Proc. Int. Conf. Inform. Network*, 2012, vol. 46, pp. 354–357.